symmetry

MDPI

Article

Computational Fluid Dynamics Based Kriging Prediction on Flutter Derivatives of Flat Steel Box Girders

Jinhua Li [1], Zhan Quan [1], Yao Zhang [1], Liyuan Cao [2] and Chunxiang Li [2,*]

1 School of Civil Engineering and Architecture, East China Jiaotong University, No.808 Shuanggang St., Nanchang 330013, China; jinhua.lee@foxmail.com or jinhua@ecjtu.edu.cn (J.L.); quanzhan0224@126.com (Z.Q.); 15070050506@163.com (Y.Z.)

2 Department of Civil Engineering, School of Mechanics and Engineering Science, Shanghai University, No.333 Nanchen Road, Shanghai 200444, China; caoly@shu.edu.cn

* Correspondence: li-chunxiang@vip.sina.com or li-chx@shu.edu.cn

Abstract: An investigation on the flutter derivative prediction of flat steel box girders is carried out based on CFD simulations. Firstly, by taking the flat steel girder section of Qingshan Yangtze River Bridge as the basic section and considering its width and height as the design variables of cross-section shape, the design domain of cross-section shape is defined by controlling the possible variation range of cross-section design variables. A small number of cross-sections are selected for the calculation of aerodynamic forces by CFD simulations. Secondly, according to the aerodynamic lift and moment time-histories of these steel box girders, of which the flutter derivatives are identified by the least square method. Next, these selected cross-section shape design parameters are used as the inputs, and the flutter derivatives obtained from CFD simulations are used as the outputs to train Kriging models. To improve the prediction accuracy of Kriging models, a modified method of model training is presented. Finally, the flutter derivatives of other cross-sections in the design domain are predicted by using the trained Kriging models, and the predicted flutter derivatives are verified by CFD simulations. It is feasible to directly predict the flutter derivatives of steel box girders by Kriging models.

Keywords: flat steel box girder; flutter derivative; prediction; Kriging model; CFD; computational simulation

check for updates

Citation: Li, J.; Quan, Z.; Zhang, Y.; Cao, L.; Li, C. Computational Fluid Dynamics Based Kriging Prediction on Flutter Derivatives of Flat Steel Box Girders. *Symmetry* **2022**, *14*, 1304. https://doi.org/10.3390/sym14071304

Academic Editors: Marco Montemurro, Constantin Fetecau and Sergei D. Odintsov

Received: 4 April 2022
Accepted: 15 June 2022
Published: 23 June 2022

1. Introduction

The increasing length of the long-span bridge is one of the main characteristics that promote the technical progress in the field of bridge engineering, and the work of exploring the feasibility of super-long-spans is crucial. However, with the increase of bridge span, long-span bridges show obvious characteristics of flexibility. Under the effect of wind load, the aeroelastic phenomenon of the bridge structure is similar to that of airplane wing [1], such as flutter, buffeting, torsional divergence, and so on [2–4]. In the above aeroelastic phenomenon, flutter is a kind of divergent vibration that will cause the bridge structure's failure. The factors that affect flutter stability of long-span flexible bridges are the aerodynamic characteristics of bridge deck cross-section, bridge stiffness and damping. It is known that the deck shape determines the aerodynamic characteristics, and the geometric properties of the deck cross-section of the bridge determine the stiffness of the bridge structure. Therefore, the design of bridge deck cross-section is particularly critical in long-span bridge engineering projects. A good cross-section design can significantly improve the wind resistance of long-span bridges. Streamlined steel box girder is widely used due to its excellent aerodynamic characteristics and cross-sectional geometric properties.

At present, wind tunnel tests and CFD numerical simulations are mainly used to study the wind-induced vibration of the streamlined steel box girder. In bridge wind resistance design, the wind tunnel test is the most common method. Wind tunnel tests can obtain static three-component force coefficient, flutter derivative, aerodynamic admittance, and Strouhal. Larose et al. [5] defined the quasi-steady aerodynamic method. They analyzed the suspension bridge and cable-stayed bridge using the aeroelastic model of the whole bridge, the extended cross-section model, and the theoretical model. The results of the three models are very consistent. In order to deeply study the aerodynamic characteristics of the long-span suspension bridge and discover its main aeroelastic phenomena, Diana et al. [6] designed a new experimental device and aeroelastic model. In addition, the segmental model test was carried out by the forced vibration method and free vibration method, and the flutter derivative, admittance function, and vortex-induced vibration of the cross-section model were analyzed. In recent decades, with the development of CFD, CFD-based numerical simulation technology has become an appropriate and reliable alternative to determine the aerodynamic behaviors of bridge deck cross-sections. Some research work has explored CFD simulation technology to obtain various parameters needed for bridge design. Li et al. [7] introduced the concept of surface flutter derivatives in order to quantify the contributions from each part of the deck surface, distributed the changes of wind-induced mode characteristics to different parts of the deck surface by further derivations based on the bimodal flutter stability expressions. The CFD simulation verified the derived formulas considering the Great Belt Bridge's deck shape and dynamic characteristics. Sarwar et al. [8] used CFD simulation to study the aerodynamic characteristics of the streamlined box girder, analyzed the flow disturbance of the girder surface, and discussed the influence of deck shape change on the aeroelastic instability of the box girder. Mannini et al. [9] used the unsteady Reynolds-averaged Navier-Stokes to simulate the flow field around a standard bridge deck. Flow solutions independent of spatial and temporal discretization were obtained by analyzing the influence of different simulation parameters. In addition, the eddy viscosity turbulence model and algebraic Reynolds stress model were compared. Šarkić et al. [10] also used the unsteady Reynolds-averaged Navier-Stokes simulation to obtain the static coefficients and unsteady flutter derivatives of the symmetrical girder section. The numerical simulation results were verified by wind tunnel test data. The results show that CFD-based numerical simulation is a reliable method for effectively calculating bridge flutter derivatives and static coefficients. Ge and Xiang [11] introduced the self-excited force model, numerical identification of flutter derivative, and flutter analysis method in flutter instability of long-span bridges. They analyzed the thin-plate section, the H-shaped section, and the closed-box section, respectively, and explored the technique of using CFD-based numerical simulation technology in the flutter response of long-span bridges. Through numerical simulations of the flow around a box girder bridge using the discrete vortex method, Nagao et al. [12] studied the influence of the triangular edge fairing on the aerodynamic stability of the bridge and verified it through wind tunnel experiments. In fact, the CFD-based numerical simulation method has become more mature so that the influence of different cross-sectional shapes on the aerodynamic characteristics of the bridge can be studied independently of wind tunnel experiments. It is also widely used by scholars because of its accuracy and convenience compared to wind tunnel tests. However, in the initial design stage of the bridge project, engineers need to perform multiple CFD-based numerical simulation calculations in order to find the most appropriate streamlined steel box girder section. Montoya et al. [13] used the surrogate model method to train the surrogate model by feeding a small amount of deck shape parameters of the cross-section and the corresponding static three-component force coefficients. Then, the static three-component force coefficients of any cross-section can be obtained through the trained surrogate model. Finally, bridge flutter derivatives were calculated by using the quasi-static formula.

The current work on the streamlined steel box girder is focused on the influence of its shape change on flutter characteristics. Whether wind tunnel test or CFD numerical simulation, it is necessary to model and analyze all cross-sections with changes in shape to find the most reasonable streamlined steel box girder cross-section, but the workload is enormous. It is time-consuming and costly to optimize the shape of the section and the structural characteristics of the bridge to improve the aeroelastic performance of the structure. Farsani et al. [14] presented the development of indicial functions for two-dimensional bridge deck sections and discussed a new set of indicial functions predicted for the cross-section of the Great Belt Bridge. Arena et al. [15] obtained the indicial aerodynamic representation of the extracted aeroelastic derivatives from CFD simulation of the deck cross-sections of the Runyang Suspension Bridge over the Yangtze River in China.

Flutter derivatives of steel box girders can be identified through CFD numerical simulations. However, CFD is also time-consuming and costly to simulate all cross-sections with changes. Kriging prediction can improve the efficiency of obtaining flutter derivatives of steel box girders and provide convenience for the design. So, this paper studies the Kriging prediction for flutter derivatives of flat steel box girders based on CFD simulations. It is a data-driven method that is based on the Kriging model to predict flutter derivatives of the bridge deck section. In addition, a modified method of Kriging model training is presented to improve the prediction accuracy under a small number of training samples. The metamodel is trained and validated using the outcome from CFD simulations.

2. Design of Flat Steel Box Girder of Qingshan Yangtze River Bridge

Qingshan Yangtze River Bridge is a crucial project of Wuhan Fourth Ring Road crossing the Yangtze River. The bridge's total length is 1638 m, the main span is 938 m, and its span layout is arranged as (100 + 102 + 148 + 938 + 148 + 102 + 100) m, as shown in Figure 1. At present, the Qingshan Yangtze River Bridge is the largest full-floating cable-stayed bridge in the world. It has the world's tallest A-type concrete bridge towers with a height of 279.5 m and fan-shaped double-cable planes. The main girder of the bridge adopts an integral flat steel box girder, and the cross-sectional geometry is shown in Figure 2. The total width of the steel box girder cross-section B = 48 m, which is the widest bridge across the Yangtze River. The height at the centerline of the box girder is H = 4.5 m. Since the Tacoma Bridge was destroyed by wind, the wind-resistant research of large-span flexible bridges has attracted much attention. This paper will take the section of the flat steel box girder of Qingshan Yangtze River Bridge as the basic section and establish a sample set of cross-sections by scaling its width and height in a certain proportion so as to develop the research on the prediction of flat steel box girder's flutter derivatives.

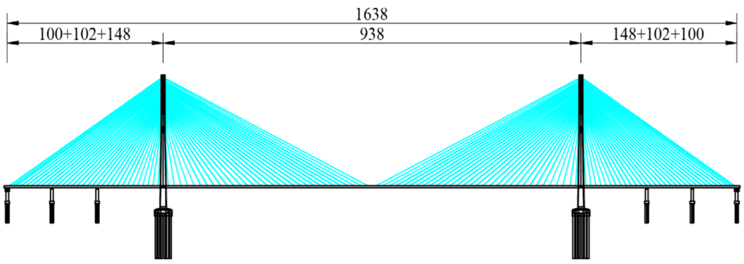

Figure 1. Elevation layout of Qingshan Yangtze River Bridge (Unit: m).

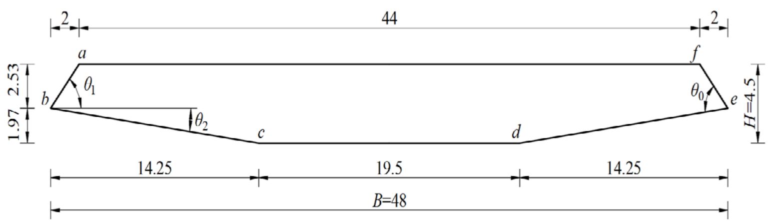

Figure 2. Flat steel box girder cross-section of Qingshan Yangtze River Bridge (Unit: m).

In this paper, the main girder cross-section of the Qingshan Yangtze River Bridge is used as the base section S_2 with the width B = 48 m. As shown in Figure 3, the width variate is ΔB, and the relative width variate of the section is $\delta_B = \Delta B/B$, namely the width variation rate of the flat steel box girder section. The section height parameter δ_H is defined in the same way. Furthermore, considering that the investigated cross-section shapes should conform to the actual cross-section requirements of the main girder, this paper sets three constant cross-section shape parameters. The width of the top plate is 44 m, the width of the bottom plate is 19.5 m, and the vertical height of the nozzle tips e and b from the top plate is 2.53 m. As shown in Figure 3, the red dotted line is the cross-sectional profile considering δ_B = +10% and δ_H = +10%, and the blue dotted line is the cross-sectional profile considering δ_B = −2.5% and δ_H = −2.5%. A reasonable range of parameters δ_B and δ_H is considered from −2.5% to +10%. As shown in Figure 4, a flat steel box girder cross-section with parameters δ_B and δ_H is expressed as a sample parameter point (δ_B, δ_H). By changing the parameters δ_B and δ_H, 19 flat steel box girder cross-sections are established as the investigated objects. In Figure 4, the flutter derivatives of the steel box girder cross-sections corresponding to the blue and black points will be used to create the Kriging models. In addition, the flutter derivatives of the steel box girder cross-sections corresponding to the red points will be compared with the flutter derivatives predicted by the Kriging models. The size of each cross-section is shown in Table 1. The maximum section width is 52.8 m, and the minimum is 46.8 m. The maximum section height is 4.95 m, and the minimum is 4.3875 m. The maximum of section air nozzle angle θ_0 is 70.8°, and the minimum is 36.12°.

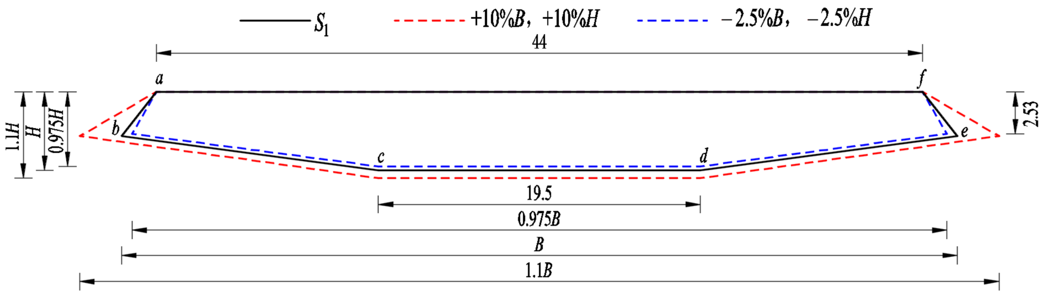

Figure 3. Section design of flat steel box girders (Unit: m).

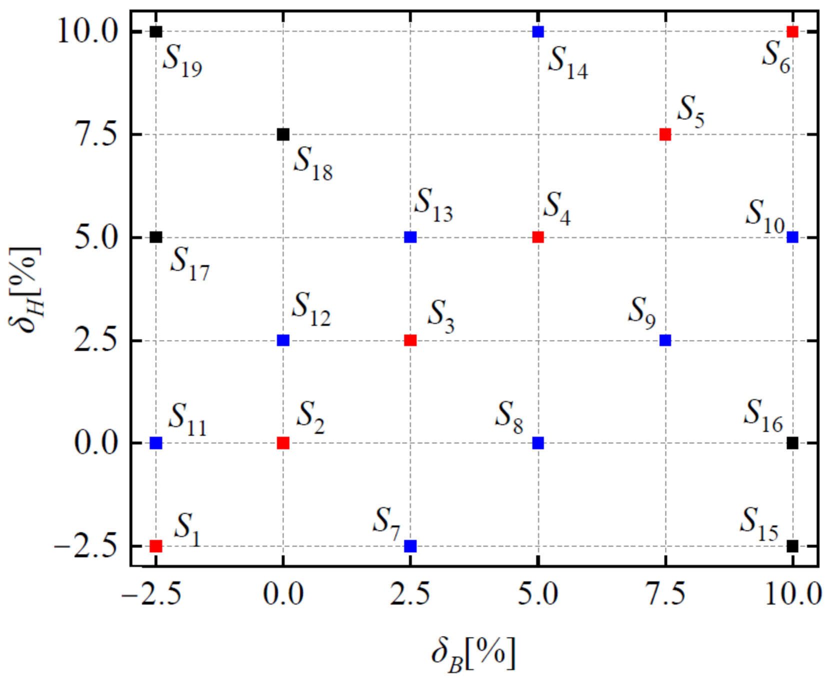

Figure 4. Variation rates of section width and height of flat steel box girders.

Table 1. Section sizes of flat steel box girder.

Girder Sections	Sizes			Angles		
	B **[m]**	***H*** **[m]**	***B/H***	$\boldsymbol{\theta_1}$ **[°]**	$\boldsymbol{\theta_2}$ **[°]**	$\boldsymbol{\theta_0}$ **[°]**
S_1	46.8	4.3875	10.67	61.10	7.47	68.57
S_2	48	4.5	10.67	51.74	7.60	59.34
S_3	49.2	4.6125	10.67	38.39	7.82	46.21
S_4	50.4	4.725	10.67	38.39	7.82	46.21
S_5	51.6	4.8375	10.67	33.71	7.93	41.64
S_6	52.8	4.95	10.67	29.95	8.03	37.98
S_7	49.2	4.3875	11.21	44.28	6.89	51.17
S_8	50.4	4.5	11.20	38.39	7.03	45.42
S_9	51.6	4.6125	11.19	33.71	7.16	40.87
S_{10}	52.8	4.725	11.18	29.95	7.29	37.24
S_{11}	46.8	4.5	10.40	61.10	7.92	69.02
S_{12}	48	4.6125	10.41	51.74	8.03	59.77
S_{13}	49.2	4.725	10.41	44.28	8.13	52.41
S_{14}	50.4	4.95	10.18	38.39	8.62	47.01
S_{15}	52.8	4.3875	12.03	29.95	6.17	36.12
S_{16}	52.8	4.5	11.73	29.95	6.55	36.50
S_{17}	46.8	4.725	9.91	61.10	8.81	69.91
S_{18}	46.8	4.95	9.45	61.10	9.70	70.80
S_{19}	48	4.8375	9.92	51.74	8.89	60.63

3. CFD Based Flutter Derivative Identification

3.1. Identification Method of Flutter Derivatives

In structural health monitoring [16–18], it is very important to carry out structural parameter identification. The frequency-domain description of aerodynamic loads is a suitable framework for studying flutter. Scanlan and Tomko [19] first proposed the aeroelastic derivatives for evaluating the flutter velocity by solving the complex eigenvalue problem. The critical condition of the problem is the state of the complex conjugate pair of eigenvalues passing through the imaginary axis [20,21]. The computation of the flutter derivatives was carried out by the classical method. The identification methods of aerodynamic derivative tests can be divided into the free vibration method [22] and the forced vibration method [6] according to the vibration of the model in the wind tunnel test. The computational fluid dynamics method used to calculate the aerodynamic derivatives of flat plates took an essential step of a numerical wind tunnel. Subsequently, scholars put forward new theories and methods to make the numerical wind tunnel develop rapidly. Cui and Chen [23] identified eight flutter derivatives of bridge section based on FLUENT and the forced vibration identification method. The results were consistent with the wind tunnel experiment, thus verifying the feasibility of the numerical method. These derivatives affect the bridge's aeroelastic behavior. So, in order to improve the aeroelastic performance of the structure, the section shape and structural characteristics of the bridge should be optimized.

Scanlan and Tomko [19] expressed the aerodynamic self-excited force as a linear function of the state vector (h, α, $\dot{h}$, $\dot{\alpha}$) by introducing eight dimensionless aerodynamic derivatives H_i^* and A_i^* (i = 1, 2, 3, 4), while ignoring the influence of the nonlinear residual term, and obtained:

$$L = \frac{1}{2}\rho U^2 (2B)\left(KH_1^*\frac{\dot{h}}{U} + KH_2^*\frac{B\dot{\alpha}}{U} + K^2H_3^*\alpha + K^2H_4^*\frac{h}{U}\right) \quad (1)$$

$$M = \frac{1}{2}\rho U^2 (2B^2)\left(KA_1^*\frac{\dot{h}}{U} + KA_2^*\frac{B\dot{\alpha}}{U} + K^2A_3^*\alpha + K^2A_4^*\frac{h}{U}\right) \quad (2)$$

where ρ is the air density; U is the incoming flow velocity; B is the width of the flat steel box girder; $K = \omega B/U$ is the converted frequency, ω is the circular frequency of vibration; h and α are the vertical bending and torsional displacement of the main beam, respectively; $\dot{h}$ and $\dot{\alpha}$ are the vertical velocity and torsional angular velocity of the girder, respectively; H_i^* and A_i^* (i = 1~4) are the flutter derivatives. The flutter derivatives are related to the shape of the girder cross-section and the converted wind speed $V_r = U/fB$, where f is the motion frequency.

In the flow field, the cross-section is forced to vibrate vertically with a single degree of freedom. The forced vertical motion expression is $h = h_0 \sin(\omega t)$, where h_0 is the vertical motion amplitude. Then, the aerodynamic lift L_i and aerodynamic lift moment M_i can be obtained according to Formulas (1) and (2). The flutter derivatives associated with vertical motion are only H_1^*, H_4^*, A_1^* and A_4^*. At each time point t_i, the residuals of the fitted values of L_i and M_i are,

$$\delta(L)_i = L_i - \frac{1}{2}\rho U^2(2B)\left(KH_1^*\frac{\dot{h}_i}{U} + K^2H_4^*\frac{h_i}{B}\right) \tag{3}$$

$$\delta(M)_i = M_i - \frac{1}{2}\rho U^2(2B)\left(KA_1^*\frac{\dot{h}_i}{U} + K^2A_4^*\frac{h_i}{B}\right) \tag{4}$$

The sum of squares of fitting residuals at N time points is,

$$\Delta_L^2 = \sum_{i=1}^{N}\left[L_i - \frac{1}{2}\rho U^2(2B)\left(KH_1^*\frac{\dot{h}_i}{U} + K^2H_4^*\frac{h_i}{B}\right)\right]^2 \tag{5}$$

$$\Delta_M^2 = \sum_{i=1}^{N}\left[M_i - \frac{1}{2}\rho U^2(2B)\left(KA_1^*\frac{\dot{h}_i}{U} + K^2A_4^*\frac{h_i}{B}\right)\right]^2 \tag{6}$$

According to the principle of least squares, in order to minimize the sum of squares of the fitting residuals, the following conditions should be satisfied.

$$\frac{\partial\Delta_L^2}{\partial H_1^*} = 0,\ \frac{\partial\Delta_L^2}{\partial H_4^*} = 0 \tag{7}$$

$$\frac{\partial\Delta_L^2}{\partial A_1^*} = 0,\ \frac{\partial\Delta_L^2}{\partial A_4^*} = 0 \tag{8}$$

The equations of H_1^*, H_4^*, A_1^* and A_4^* are expressed as follows,

$$\rho B^2\omega\begin{pmatrix} \sum\limits_{i=1}^{N}\dot{h}_i^2 & \omega\sum\limits_{i=1}^{N}h_i\dot{h}_i \\ \omega\sum\limits_{i=1}^{N}\dot{h}_ih_i & \omega\sum\limits_{i=1}^{N}h_i^2 \end{pmatrix}\begin{pmatrix} H_1^* & A_1^* \\ H_4^* & A_4^* \end{pmatrix} = \begin{pmatrix} \sum\limits_{i=1}^{N}L_i\dot{h}_i & \sum\limits_{i=1}^{N}M_i\dot{h}_i \\ \sum\limits_{i=1}^{N}L_ih_i & \sum\limits_{i=1}^{N}M_ih_i \end{pmatrix} \tag{9}$$

The flutter derivatives H_1^*, H_4^*, A_1^* and A_4^* are obtained by solving this system of equations. Increasing the wind speed U step by step, the curves of 4 flutter derivatives changing with the converted wind speed V_r can be obtained.

Similarly, letting the cross-section model do torsional single-degree-of-freedom forced vibration $\alpha = \alpha_0\sin(\omega t)$, other four flutter derivatives such as H_2^*, H_3^*, A_2^* and A_3^* related to torsional motion can be obtained.

3.2. Flow Field Meshing of Qingshan Yangtze River Bridge

According to the selected 19 flat steel box girder sections, the CFD-based calculation models are established, respectively. As shown in Figure 5, for a steel box girder section with the width B, the calculation basin of the model is set as a rectangular area of $25B \times 20B$. The distance from the inlet boundary to the cross-section center is $10B$, and the distance from the outlet boundary to the cross-section center is 15B. In addition, the upper and lower boundaries are 10B from the cross-section center. Using the above parameters to set the flow field can try to avoid the separation vortex rolled up at the back of the object hitting the outer boundary and reflecting back, which affects the calculation accuracy. At the same time, it also makes the flow field parameter distribution near the outer boundary compatible with the assumed boundary conditions. In this way, the convergence of calculation can be well realized.

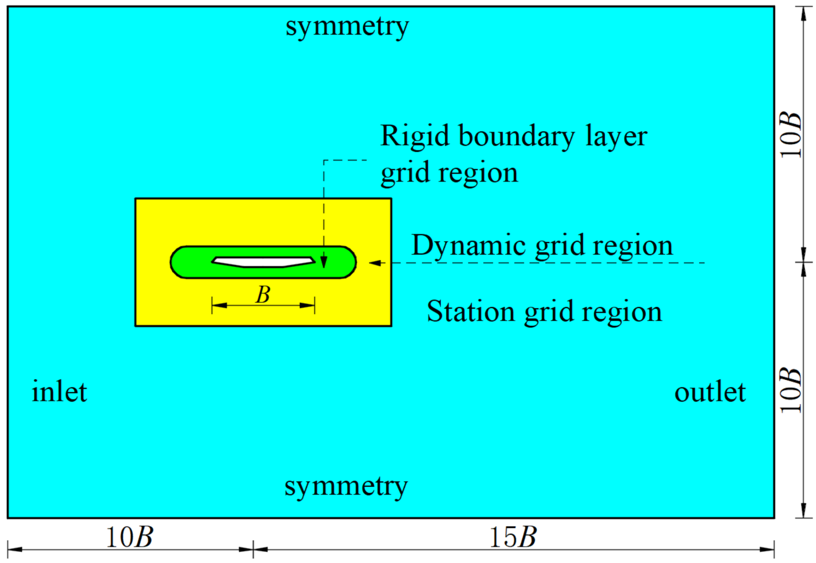

Figure 5. Division of flow field in CFD numerical simulation.

The flow field is divided into rigid boundary layer grid region, dynamic grid region, and static grid region, as shown in Figure 5. In order to meet the different functional requirements of each flow field region, this paper uses two kinds of grids to divide the flow field, namely structured grid and unstructured grid. The grid meshing of the computational flow field is shown in Figure 6. The rigid boundary layer grid region and the static grid region have many grids, and the grid size needs to be controlled to increase according to a certain proportion. Therefore, the structured quadrilateral grid is used for the two regions. The structured quadrilateral grid of the rigid boundary layer region is shown in Figure 7. The shape of the dynamic grid region changes during the calculation process, and the spring smoothing method is used in the subsequent calculations. However, the spring smoothing method can only be applied to unstructured grids. Therefore, the dynamic grid region is meshed by the unstructured triangular grid, as shown in Figure 8. In order to make the calculation result correct, for the rigid boundary layer grid region, the mesh thickness of the first layer near the wall is set to be about $1.04 \times 10^{-4}B$, and the growth factor is controlled to 1.1.

In this paper, a CFD software is used for the numerical simulation. For the simulation of wind fields, the $k-\varepsilon$ standard turbulence model was used, the turbulent viscosity ratio of inlet and outlet were 5% and 10%, respectively, and eight wind speeds from 4 m/s to 32 m/s were selected as inlet wind speeds, respectively. The calculation state is based on the Unsteady calculation, and the time step size is 0.01 s.

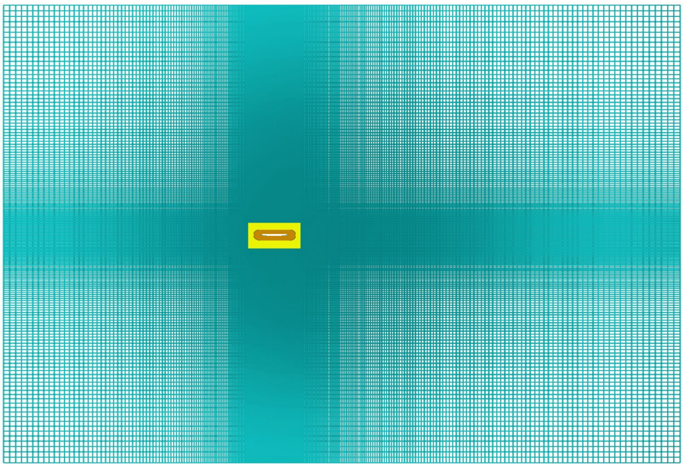

Figure 6. Meshing of the computational flow field.

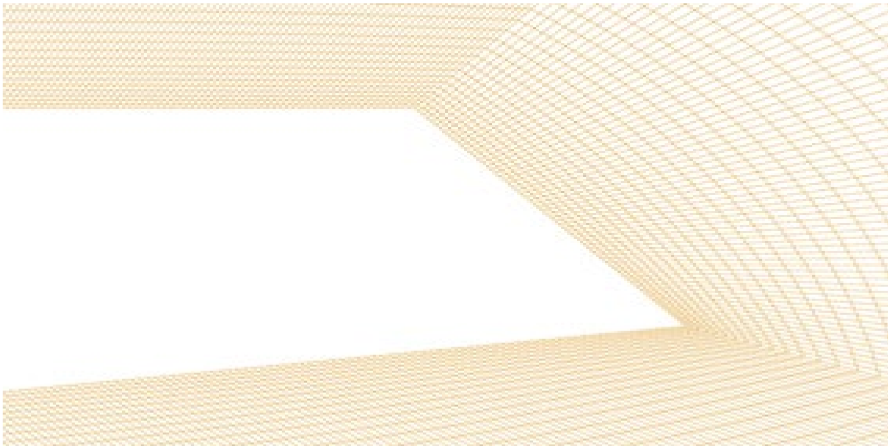

Figure 7. Structured quadrilateral grid in rigid boundary layer region.

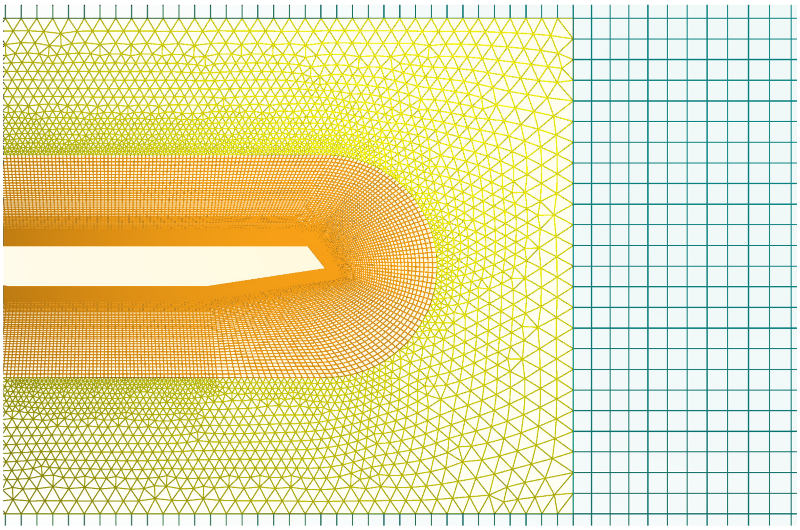

Figure 8. Unstructured triangular grid in the dynamic grid region.

3.3. Flutter Derivative Identification of Flat Steel Box Girders

After meshing the selected 19 flat steel box girder sections, CFD numerical calculations are performed on them, respectively. The turbulence model adopts the standard k-ε model, the turbulence intensity is set to 5%, and the turbulence viscosity ratio is 10. The left boundary of the flow field is set as the velocity inlet boundary, and the velocity gradient with height is zero. The right boundary is set as the pressure outlet boundary, and the gauge head pressure is zero. The upper and lower boundaries of the flow field are set to symmetry. The outer wall of the steel box girder adopts a non-slip wall boundary. By compiling user-defined functions (UDF), the rigid boundary layer is controlled to perform simple harmonic motion in the dynamic grid region. Both the spring smoothing method and the local mesh reconstruction method are used to update the dynamic grid.

By forcing the steel box girders to do simple harmonic vibration as $h_i = h_0 \sin(\omega t_i)$ with the amplitude h_0 = 0.02 m and the time step t_i= 0.01 s, the aerodynamic time history of each flat steel box girder is calculated under various wind speeds. Taking the wind speed of 4 m/s as an example, the forced vibration of a steel box girder S_2 will arouse fluid movement in the surrounding flow field. As shown in Figure 9, by observing the wind speed distribution of the flow field at time nodes $T/4$, $T/2$, $3T/4$, T of a period time T, it is found that the wake swings together with the steel box girder. With the streamlined aerodynamic shape of the cross-section, there is no apparent vortex shedding in the wake. Moreover, taking eight wind speeds from 4 m/s to 32 m/s, respectively, the corresponding aerodynamic steady responses of the flat steel box girder are shown in Figure 10.

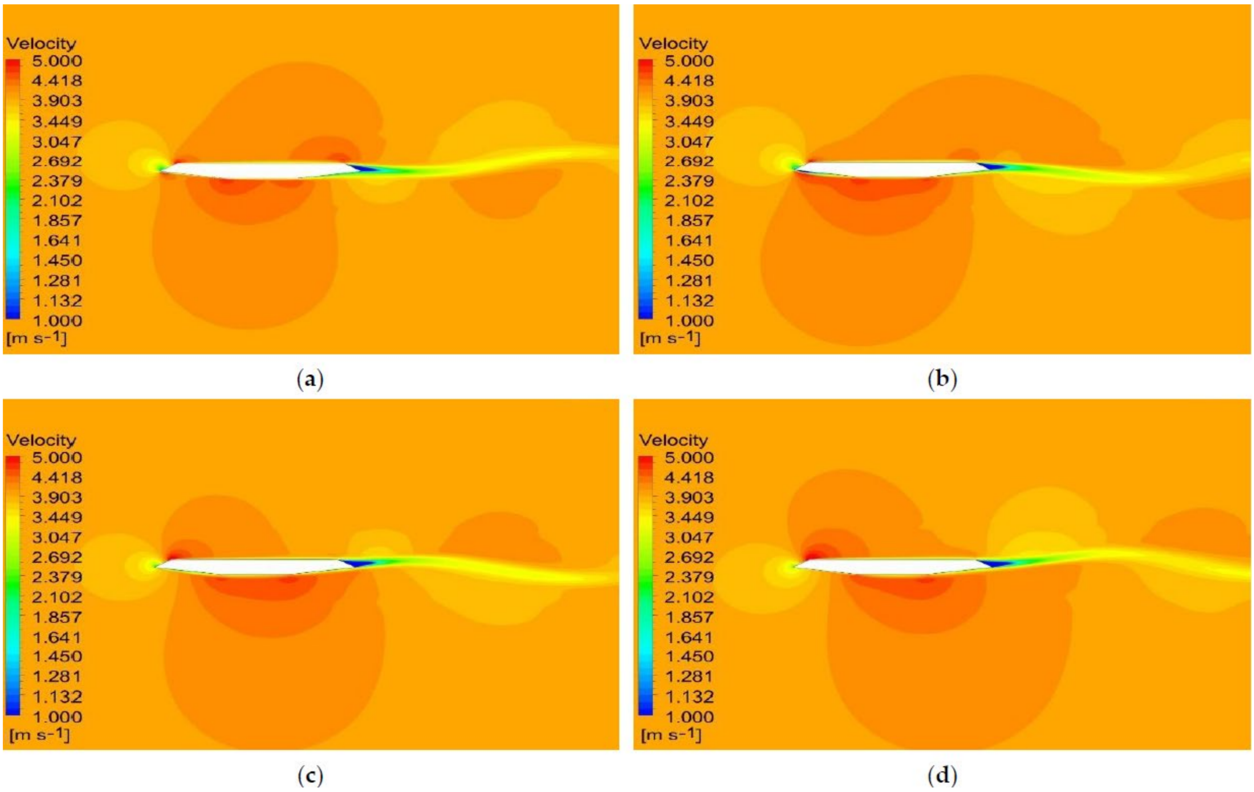

Figure 9. Wind speed field around a steel box girder S_2 with a vertical motion under 4 m/s wind speed: (**a**) $t = T/4$; (**b**) $t = T/2$; (**c**) $t = 3T/4$; (**d**) $t = T$.

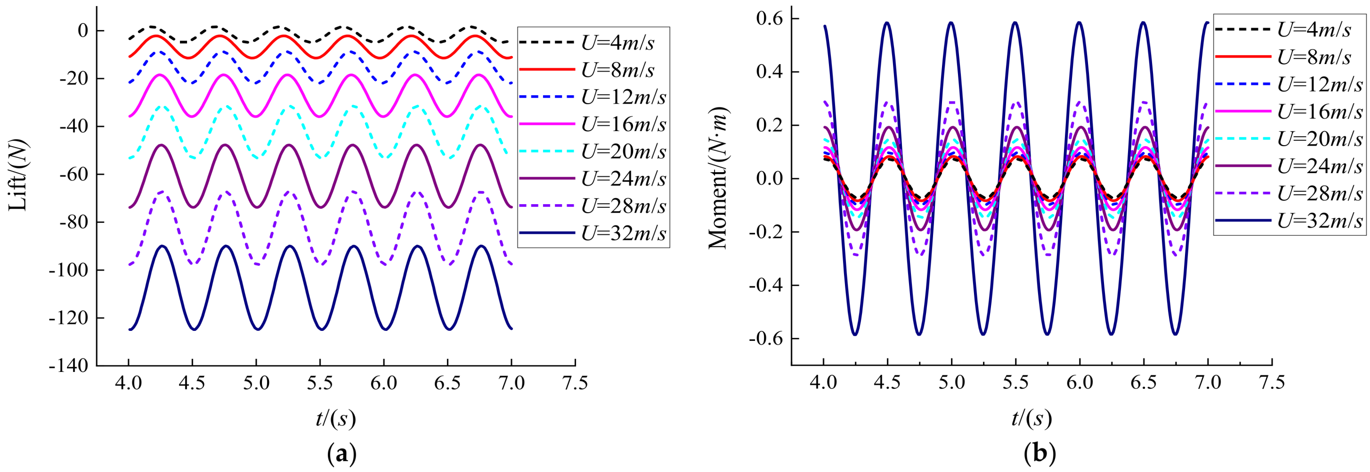

Figure 10. Aerodynamic forces of a steel box girder S_2 with a vertical motion under different wind speeds: (**a**) Aerodynamic lift; (**b**) Aerodynamic moment.

Figure 10a shows the lift of the thin plate under vertical forced vibration at various incoming wind speeds. The mean lift time history of the thin plate decreases with the increase of incoming wind speed, which is caused by the negative lift coefficient of the thin plate at a zero angle of attack. Figure 10b is the time history of the moment of the thin plate under vertical forced vibration at various incoming wind speeds. The mean torque time history of the thin plate is about zero, but its amplitude increases with the increase of incoming wind speed. Since the vibration frequency of lift and moment time histories is determined by the force motion frequency, the frequency of lift, lift moment, and forced displacement time histories are the same.

In the same way, by forcing the investigated steel box girders to do simple harmonic torsional vibration as $a_i = a_0 \sin(\omega t_i)$ with the amplitude $a_0 = 2\pi/180$, the aerodynamic forces of each flat steel box girder are also calculated at various wind speeds. Similarly, under 4 m/s wind speed, the wind speed field around the steel box girder S_2 undergoing torsional forced motion in a period T is shown in Figure 11. With the torsional forced motion of the cross-section model, the wind speed field changes significantly. Under various wind speeds, the time history of aerodynamic forces on the steel box girder undergoing torsional forced motion can be obtained, as shown in Figure 12. Figure 12a is the lift time history of the thin plate under torsional forced vibration at various incoming wind speeds. The fluctuation of the lift time history of the thin plate increases significantly compared with Figure 10a because the forced torsional motion changes the initial attack angle of the thin plate. Figure 12b shows the moment of the thin plate under torsional forced vibration at various incoming wind speeds. Its amplitude increases significantly compared with that in Figure 10b, which is also caused by the initial attack angle of the thin plate caused by torsional forced motion.

Then, according to the above flutter derivative identification method, the eight flutter derivatives of the flat steel box girder S_2 at various wind speeds can be obtained by fitting the aerodynamic forces, as shown in Figure 13. Similarly, the flutter derivatives of the selected 19 cross-sections at any reasonable wind speed can be obtained. The flutter derivatives of the selected 19 cross-sections at a wind speed of 4 m/s are listed in Table 2.

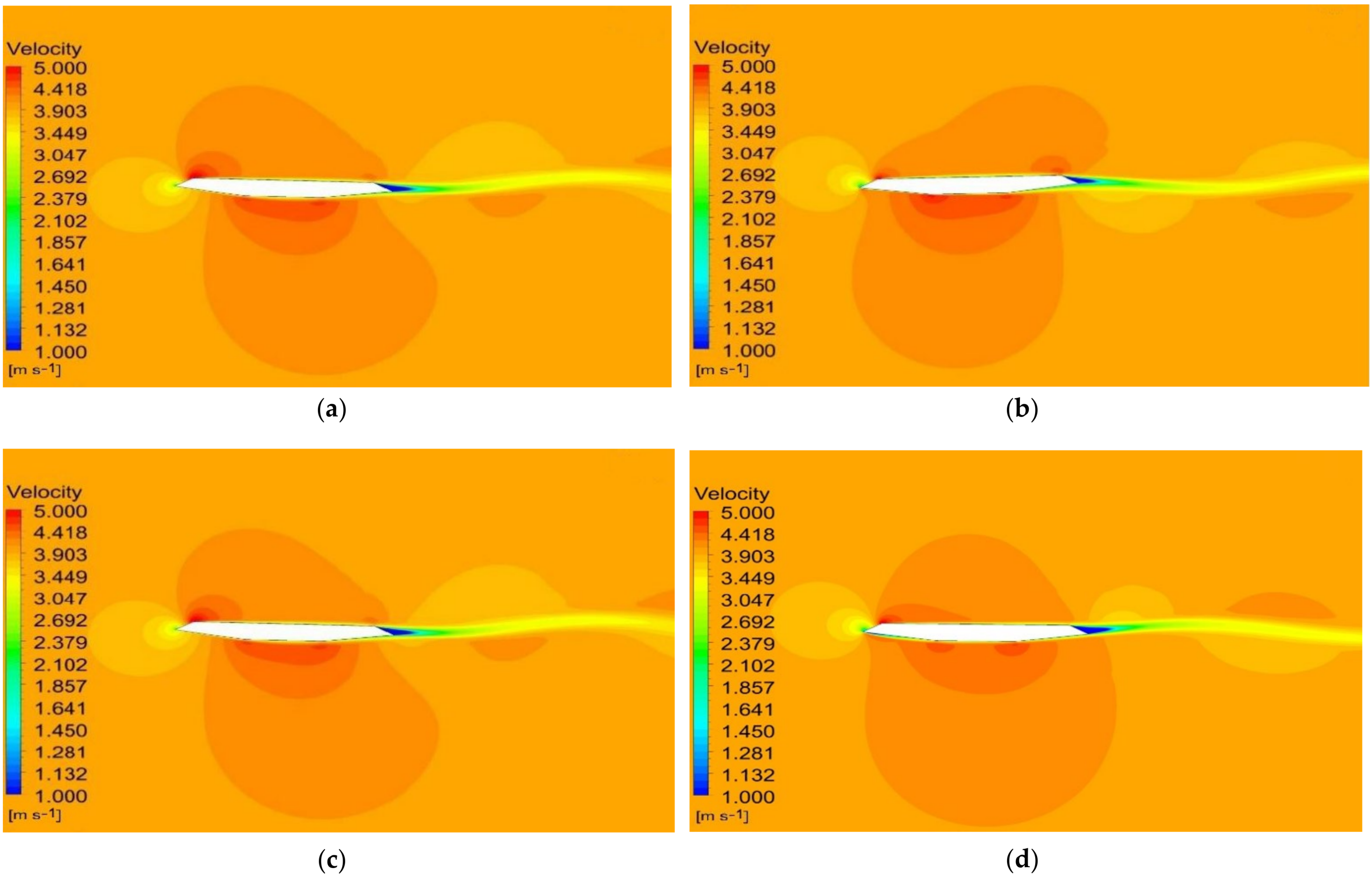

Figure 11. Wind speed field around a steel box girder S_2 with a torsion motion under 4 m/s wind speed: (**a**) $t = T/4$; (**b**) $t = T/2$; (**c**) $t = 3T/4$; (**d**) $t = T$.

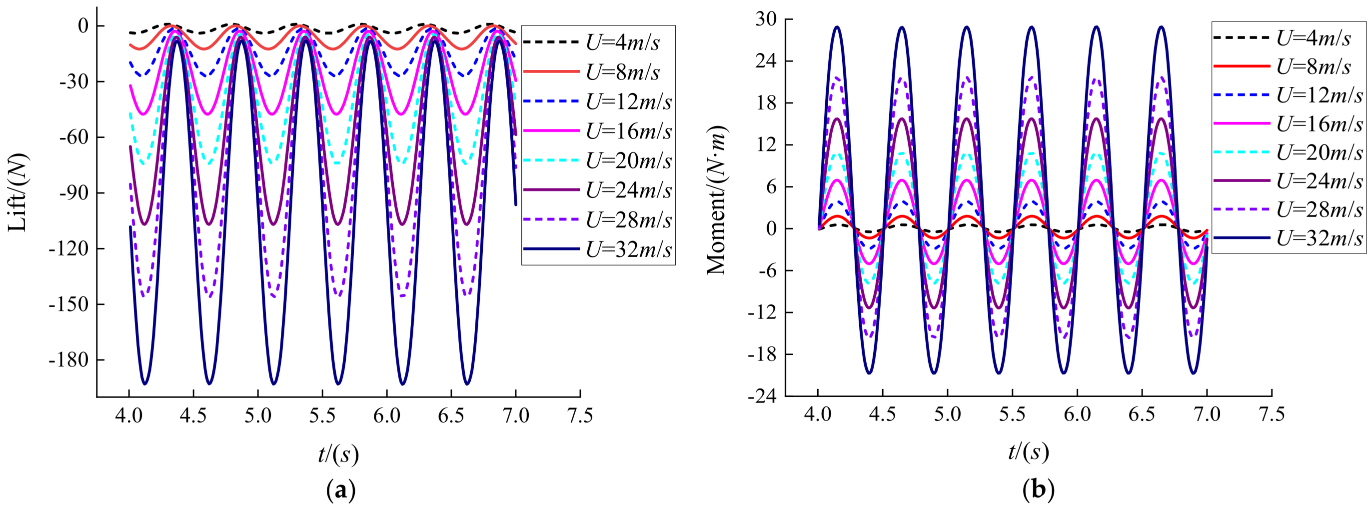

Figure 12. Aerodynamic forces of a steel box girder S_2 with a torsion motion under different wind speeds: (**a**) Aerodynamic lift; (**b**) Aerodynamic moment.

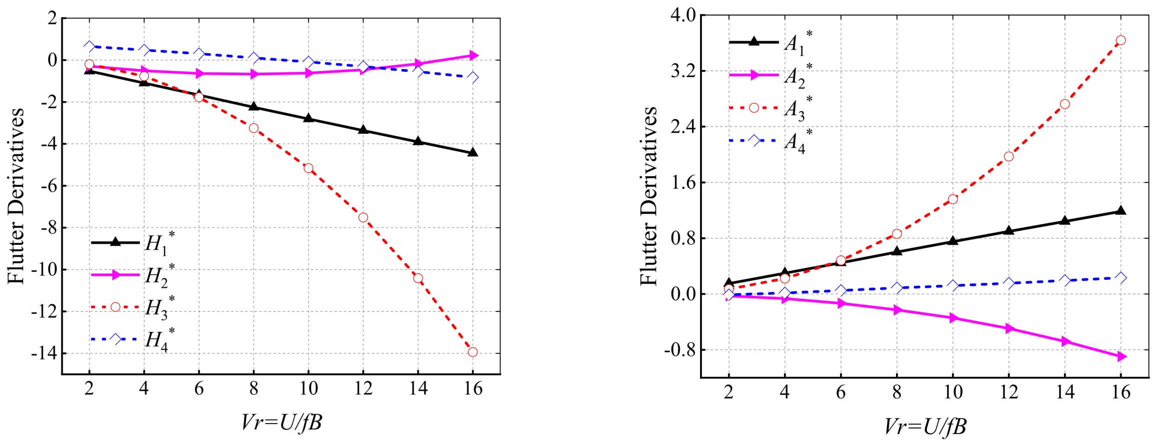

(**a**) (**b**)

Figure 13. Flutter derivatives of a flat steel box girder S_2 under different wind speedss: (**a**) H_1^*, H_2^*, H_3^*, H_4^*; (**b**) A_1^*, A_2^*, A_3^*, A_4^*.

Table 2. Flutter derivatives of 19 flat steel box girders under 4 m/s *wind* speed.

Girder Sections	Flutter Derivatives							
	H_1^*	H_2^*	H_3^*	H_4^*	A_1^*	A_2^*	A_3^*	A_4^*
S_1	−0.5373	−0.2996	−0.2037	0.6642	0.1536	−0.0295	0.0715	−0.0067
S_2	−0.5272	−0.2957	−0.1992	0.6480	0.1511	−0.0272	0.0706	−0.0090
S_3	−0.5135	−0.2937	−0.1866	0.6427	0.1514	−0.0237	0.0674	−0.0111
S_4	−0.4971	−0.2814	−0.1880	0.6281	0.1502	−0.0238	0.0700	−0.0131
S_5	−0.4847	−0.2826	−0.1814	0.6147	0.1502	−0.0215	0.0697	−0.0126
S_6	−0.4616	−0.2750	−0.1702	0.6097	0.1507	−0.0202	0.0702	−0.0141
S_7	−0.5274	−0.2898	−0.1959	0.6370	0.1506	−0.0252	0.0709	−0.0096
S_8	−0.5139	−0.2906	−0.1884	0.6241	0.1500	−0.0248	0.0704	−0.0110
S_9	−0.4920	−0.2826	−0.1833	0.6168	0.1450	−0.0224	0.0701	−0.0125
S_{10}	−0.4682	−0.2780	−0.1718	0.6120	0.1510	−0.0207	0.0706	−0.0133
S_{11}	−0.5306	−0.2973	−0.2020	0.6612	0.1538	−0.0289	0.0713	−0.0077
S_{12}	−0.5988	−0.2939	−0.1979	0.6445	0.1513	−0.0266	0.0705	−0.0099
S_{13}	−0.5185	−0.2898	−0.1959	0.6310	0.1501	−0.0252	0.0699	−0.0110
S_{14}	−0.4811	−0.2820	−0.1883	0.6215	0.1518	−0.0248	0.0690	−0.0130
S_{15}	−0.4774	−0.2825	−0.1752	0.6192	0.1517	−0.0215	0.0712	−0.0122
S_{16}	−0.4448	−0.2789	−0.1717	0.6140	0.1512	−0.0206	0.0710	−0.0131
S_{17}	−0.5242	−0.2947	−0.1993	0.6562	0.1526	−0.0278	0.0707	−0.0090
S_{18}	−0.5134	−0.2895	−0.1943	0.6377	0.1501	−0.0254	0.0697	−0.0110
S_{19}	−0.5176	−0.2915	−0.1970	0.6483	0.1522	−0.0270	0.0701	−0.0100

4. Kriging Prediction on Flutter Derivatives of Steel Box Girders

In the bridge design stage, the shape parameter design of the main girder cross-section is the key to the bridge wind resistance design. Many CFD numerical models or wind tunnel experimental models must be constructed to find the optimal wind resistance cross-section of the main girder by using traditional methods. So, the design of the main girder cross-section is an optimization process. This process is very time-consuming, and the optimization direction is not clear. Instead of the CFD numerical model or the wind tunnel experimental model for optimization, the surrogate model can be used to express the relationship between the cross-section design parameters and the wind-induced vibration response to improve the efficiency of the main girder parameter design. Surrogate models have also been applied in the field of wind engineering. By using surrogate modes, Chen et al. [24] generated flutter derivatives of rectangular cross-sections, and Elshaer et al. [25] simulated the aerodynamics of tall buildings' cross-sections.

At present, there are many surrogate models, such as the Kriging model [26], multiple adaptive regression spline model [27], artificial neural network model [28], and so on. In order to improve the aeroelastic performance of the structure, the shape of the bridge section must be optimized. The Kriging model may be a feasible method to enhance the efficiency of obtaining the flutter derivatives of the steel box girders. Therefore, the Kriging model predicting the flutter derivatives of the steel box girders is investigated in this paper. For the Kriging prediction of flutter derivatives of steel box girders, the Kriging model can be established by training the flutter derivatives of some main beams. The shape design variables of the steel box girder cross-section and its flutter derivatives are used as the input and output data of the Kriging model, respectively. Then, by comparing the flutter derivatives predicted by the Kriging model with those identified by CFD numerical simulations, the prediction effect of the Kriging model can be evaluated.

4.1. Kriging Prediction Method

The Kriging model is a method of interpolation in space to expand data on the spatial scale. It uses the known observations at some spatial points to estimate the variable values at other locations in space. So, it is also called space estimation Kriging. For the investigated 19 box girders, the shape parameters δ_B and δ_H of each cross-section can be taken as a coordinate point S (δ_B, δ_H) shown in Figure 4. Namely, each coordinate point (S_i, $i = 1 \sim 19$) represents a steel box girder cross-section. Then, the flutter derivatives of steel box girders are taken as the objects of the known observations and predicted values in Kriging prediction.

Therefore, given n observed values (flutter derivatives) $\mathbf{Y} = \left[f\left(S^{(1)}\right), \cdots, f\left(S^{(n)}\right)\right]^T$, the flutter derivatives of other cross-sections $S^{(m)}$ can be predicted by the Kriging correlation [29–31],

$$f\left(S^{(m)}\right) = \hat{\mu} + \boldsymbol{\Psi}^T \boldsymbol{R}^{-1}(\boldsymbol{Y} - \boldsymbol{I}\hat{\mu}) \tag{10}$$

where $\boldsymbol{I}$ is a unit column vector of $n \times 1$; the column vector $\boldsymbol{\Psi}$ of $n \times 1$ is the basis function, which is composed of the correlation function values between the predicted value $f\left(S^{(m)}\right)$ and all known observations $f\left(S^{(1)}\right), \cdots, f\left(S^{(n)}\right)$; the matrix $\boldsymbol{R}$ of $n \times n$ is composed of the correlation function values between all known observations $f\left(S^{(1)}\right), \cdots, f\left(S^{(n)}\right)$, namely the matrix element $R_{i,j} = Corr\left[f\left(S^{(i)}\right), f\left(S^{(j)}\right)\right]$; $\hat{\mu}$ is the global trend representing the mathematical expected value of $f\left(S^{(m)}\right)$, namely,

$$\hat{\mu} = \left(\frac{\boldsymbol{I}^T \boldsymbol{R}^{-1} \boldsymbol{Y}}{\boldsymbol{I}^T \boldsymbol{R}^{-1} \boldsymbol{I}}\right) \tag{11}$$

$\boldsymbol{\Psi}^T \boldsymbol{R}^{-1}(\boldsymbol{Y} - \boldsymbol{I}\hat{\mu})$ represents a static random process with zero mean and variance σ^2, which the maximum likelihood estimator can obtain,

$$\hat{\sigma}^2 = \frac{1}{n}(\boldsymbol{Y} - I\hat{\mu})^T \boldsymbol{R}^{-1}(\boldsymbol{Y} - \boldsymbol{I}\hat{\mu}) \tag{12}$$

where $\boldsymbol{R}^{-1}(\boldsymbol{Y} - \boldsymbol{I}\hat{\mu})$ represents the weight assigned to the basis function $\boldsymbol{\Psi}$, the vector element of $\boldsymbol{\Psi}$ is $\Psi_i\left(S^{(m)}\right) = Corr\left[f\left(S^{(i)}\right), f\left(S^{(m)}\right)\right]$. At present, the common correlation function is the Gaussian exponential model, and its expression is,

$$Corr\left[f(S^{(i)}), f(S^{(j)})\right] = exp\left(\sum_{k=1}^{n} \varepsilon_k \left\| S_k^{(i)} - S_k^{(j)} \right\|^{p_k}\right) \tag{13}$$

where ε_k is the kth component of the Gaussian exponential model parameter ε, and p_k is the kth component of the anisotropy parameter p, which determines the degree of smoothness.

The model parameters ε and p are determined by maximizing the so-called concentrated log-likelihood function (*CLL*), given by [31],

$$CLL = -\frac{n}{2}\ln(\hat{\sigma}^2) - \frac{1}{2}\ln(|\boldsymbol{R}|) \quad (14)$$

The derivation of the Kriging predictor as Equation (10) was shown by Jones [31] and is the most straightforward and intuitive way of explaining the way predictions are made [30].

4.2. Predicted Flutter Derivatives of Steel Box Girders

The flutter derivative prediction of steel box girder sections can be regarded as an input-output system. Namely, the objective function is a function of the design variables of the section shapes, and the Kriging models are trained by using the known input-output sample set. Then, the established Kriging models can quickly predict the steel box girder's flutter derivatives to improve the efficiency of obtaining the flutter derivatives of steel box girders. The two input variables of the Kriging models are δ_B and δ_H, which are the width and height change rates of the girder section shape, respectively. The output variable is the steel box girder's flutter derivatives. It should be noted that each steel box girder involves eight different flutter derivatives, and the corresponding Kriging models should be established for various flutter derivatives.

Under the converted wind speed Vr = 2, the flutter derivatives of the 13 steel box girder sections corresponding to the blue and black points shown in Figure 4 are selected for the Kriging model training. As shown in Figure 14, the response surface of each flutter derivative can be obtained from the Kriging model output. The response surface can reflect the variation trend of the corresponding flutter derivative in the design domain of the entire cross-sectional shapes. Apparently, the flutter derivatives H_1^*, H_2^*, H_3^* and A_2^* show an increasing trend with width and height. On the contrary, H_4^* and A_4^* decrease with the growth of width and height. Furthermore, A_1^* and A_3^* decrease first and then increase as the width increases. It can also be seen from Figure 14 that the influence of the girder width on flutter derivatives is more significant than that of the girder height because the change of the flat steel box girder's width greatly influences the aerodynamic lift and lift moment.

Similarly, the Kriging models of 8 flutter derivatives under various converted wind speeds can be trained to predict the trend of all flutter derivatives with the converted wind speeds. These Kriging models trained by flutter derivatives of 13 steel box girder sections $S_7 \sim S_{19}$ are named Kriging1. In order to show the Kriging prediction effect, the prediction results are compared with the results from the CFD numerical simulation. The flutter derivatives of the girder section S_2 under different converted wind speeds are displayed in Figure 15. The flutter derivatives of the girder section S_2 predicted by Kriging1 are very consistent with the CFD results. Furtherly, the flutter derivatives of 8 steel box girder sections $S_7 \sim S_{14}$ corresponding to the blue points in Figure 4 are selected for Kriging model training. These trained Kriging models are taken as Kriging2. As shown in Figure 15, The flutter derivatives of the girder section S_2 predicted by Kriging2 are also in good agreement with the CFD results. So, it is feasible to predict the flutter derivatives of steel box girders by Kriging prediction.

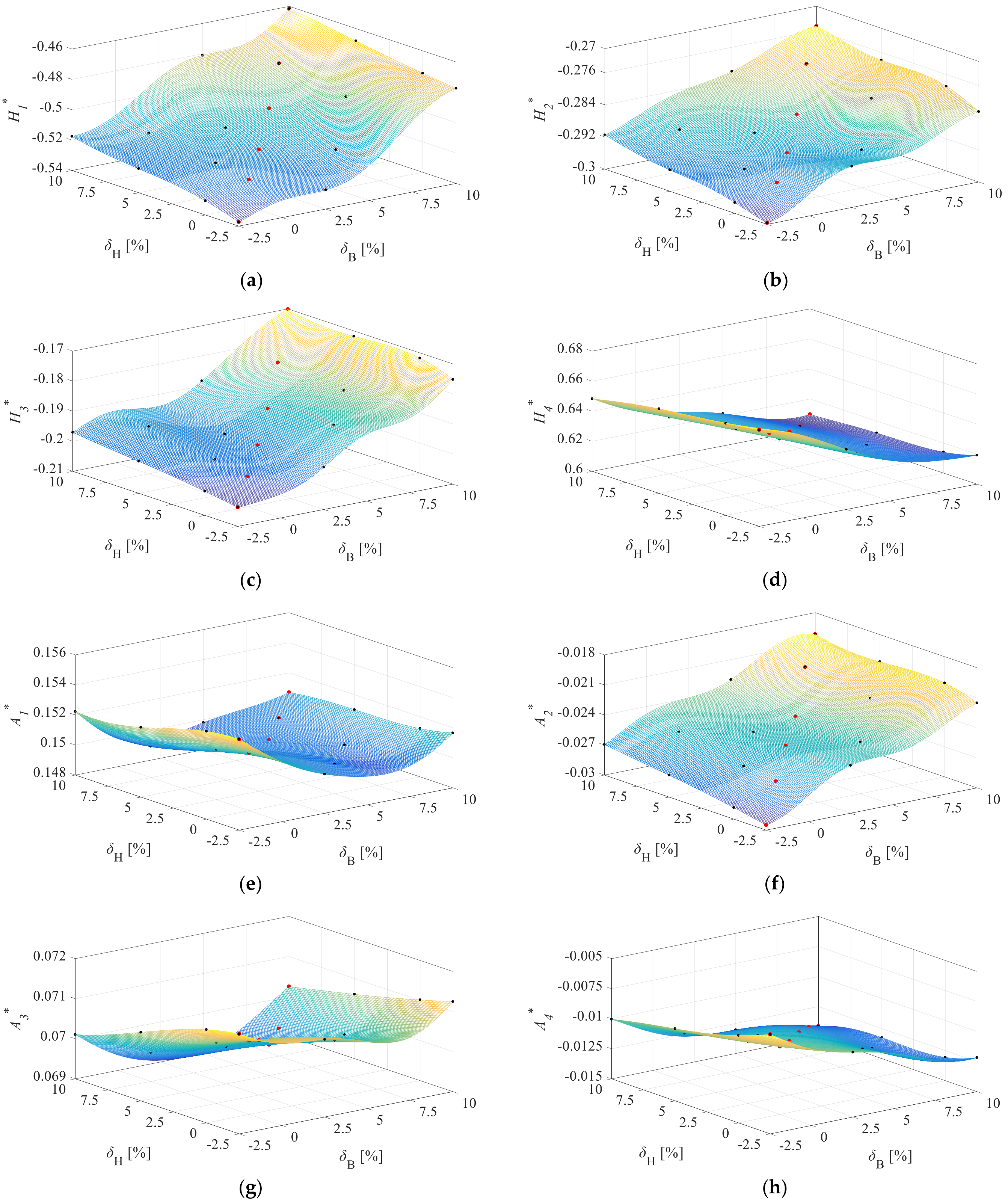

Figure 14. The response surfaces of 8 flutter derivatives from the Kriging model output under $Vr = 2$: (**a**) H_1^*; (**b**) H_2^*; (**c**) H_3^*; (**d**) H_4^*; (**e**) A_1^*; (**f**) A_2^*; (**g**) A_3^*; (**h**) A_4^*.

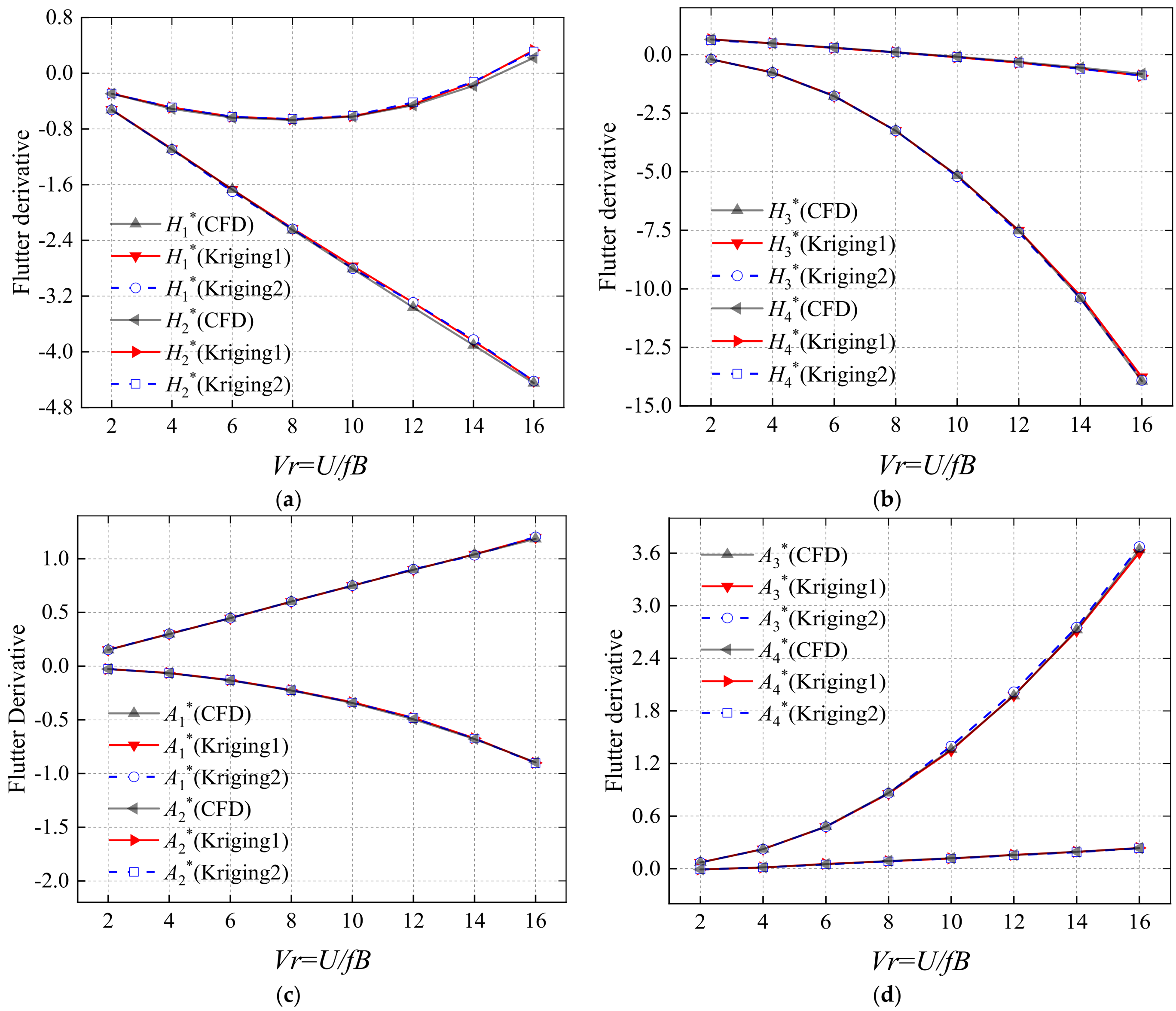

Figure 15. The flutter derivatives of the steel box girder section S_2 under different converted wind speeds: (**a**) H_1^*, H_2^*; (**b**) H_3^*, H_4^*; (**c**) A_1^*, A_2^*; (**d**) A_3^*, A_4^*.

Due to the number reduction of training samples of flutter derivatives of steel box girders, the error of Kriging2 is more than Kriging1, although the consuming time of Kriging2 is less than Kriging1. In this paper, a modified method for model training is presented to improve the prediction accuracy of Kriging2. According to some steel box girder sections (S_7~S_{14}) with known flutter derivatives, the sections with unknown flutter derivatives are selected as the predicted girder sections. For ensuring better prediction results, the predicted girder sections (such as S_2 and S_3 in Figure 4) need to be surrounded by more steel box girders with known flutter derivatives. Secondly, the Kriging models are trained by the known flutter derivatives to predict the flutter derivatives of the selected girder section. Finally, the predicted flutter derivatives of the girder section are taken as new known flutter derivatives, and the first step is returned. Through the above method, the predicted flutter derivatives of each steel box girder can be modified. The accuracy of Kriging models in predicting flutter derivatives of steel box girder sections is further analyzed. As shown in Figures 16 and 17, the flutter derivatives of steel box girder sections $S_1 \sim S_6$ under the converted wind speed Vr = 2 are predicted by Kriging1, Kriging2 and modified Kriging2. In the modified Kriging2, the flutter derivatives of girder sections from S_1 to S_6 are predicted by the updated kriging models in turn.

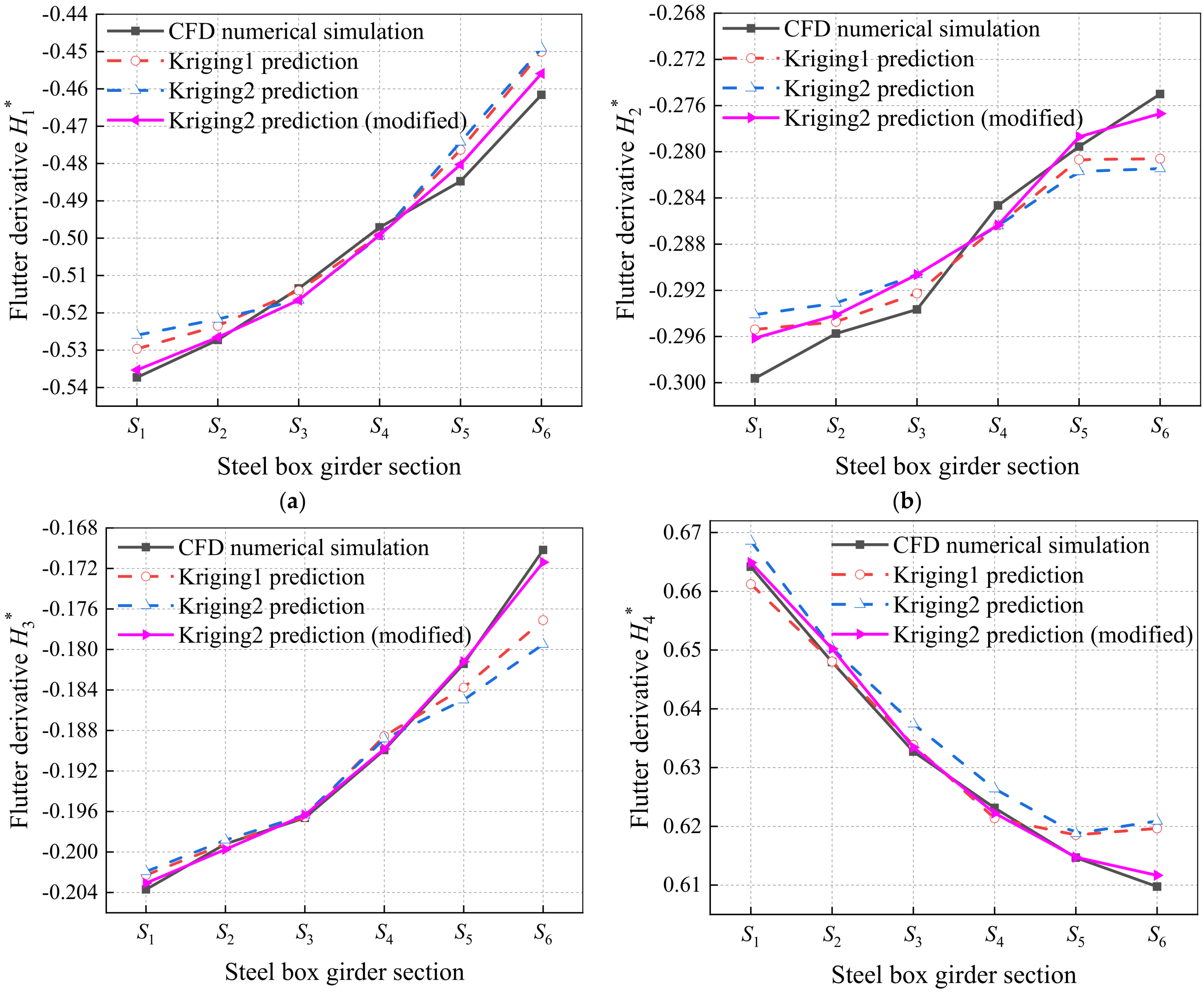

Figure 16. The flutter derivatives H_1^*, H_2^*, H_3^* and H_4^* of the steel box girder sections S_1~S_6 under Vr = 2: (**a**) H_1^*; (**b**) H_2^*; (**c**) H_3^*; (**d**) H_4^*.

It can be seen from Figures 16 and 17 that compared with Kriging2 prediction, Kriging1 prediction for the flutter derivatives of steel box girder sections is closer to the CFD numerical simulation. The reason is that Kriging1 prediction has more training samples than Kriging2 prediction. However, Kriging2 prediction can be improved by the modified method of Kriging model training, which repeatedly takes the predicted flutter derivatives of Kriging2 to increase the training samples of the model and update the trained Kriging models. As shown in Figures 16 and 17, the modified Kriging2 prediction is superior to the Kriging2 prediction. Even for some girder sections such as S_1, S_5 and S_6, it is closer to the CFD numerical simulation than the Kriging1 prediction. The errors of flutter derivatives predicted by Kriging1, Kriging2 and modified Kriging2 are shown in Figure 18. The flutter derivative errors of S_1, S_5 and S_6 are significantly larger than those of S_2, S_3 and S_4. The reason is that the girder sections (such as S_7~S_{19} in Figure 4) used to train Kriging models are not evenly distributed in the girder section design domain. Obviously, the errors increase with the decrease of training samples from S_7~S_{19} to S_7~S_{14}. However, the modified method of Kriging model training can effectively improve the prediction accuracy under a small number of training samples.

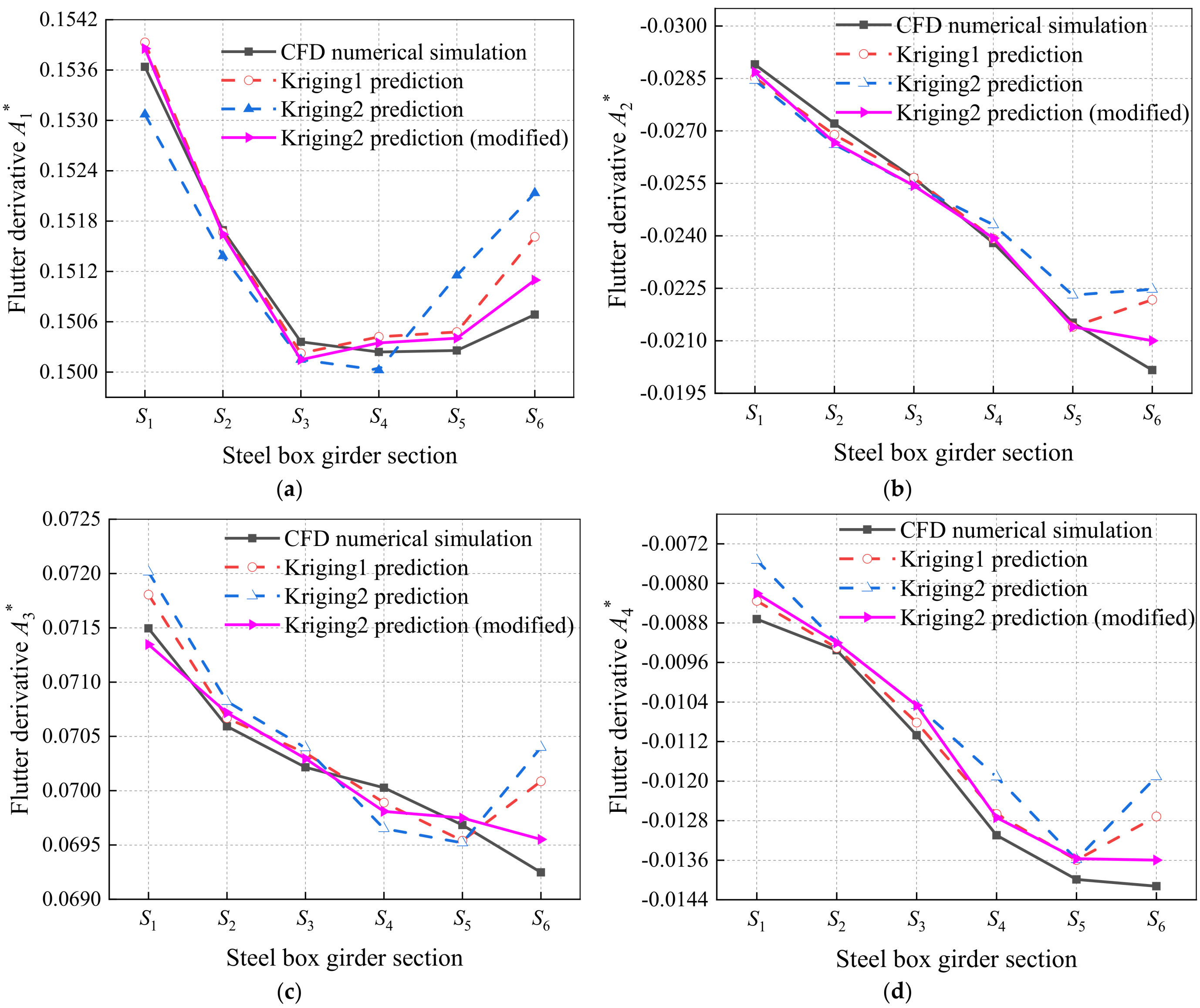

Figure 17. The flutter derivatives A_1^*, A_2^*, A_3^* and A_4^* of the steel box girder sections S_1 ~ S_6 under Vr = 2: (**a**) A_1^*; (**b**) A_2^*; (**c**) A_3^*; (**d**) A_4^*.

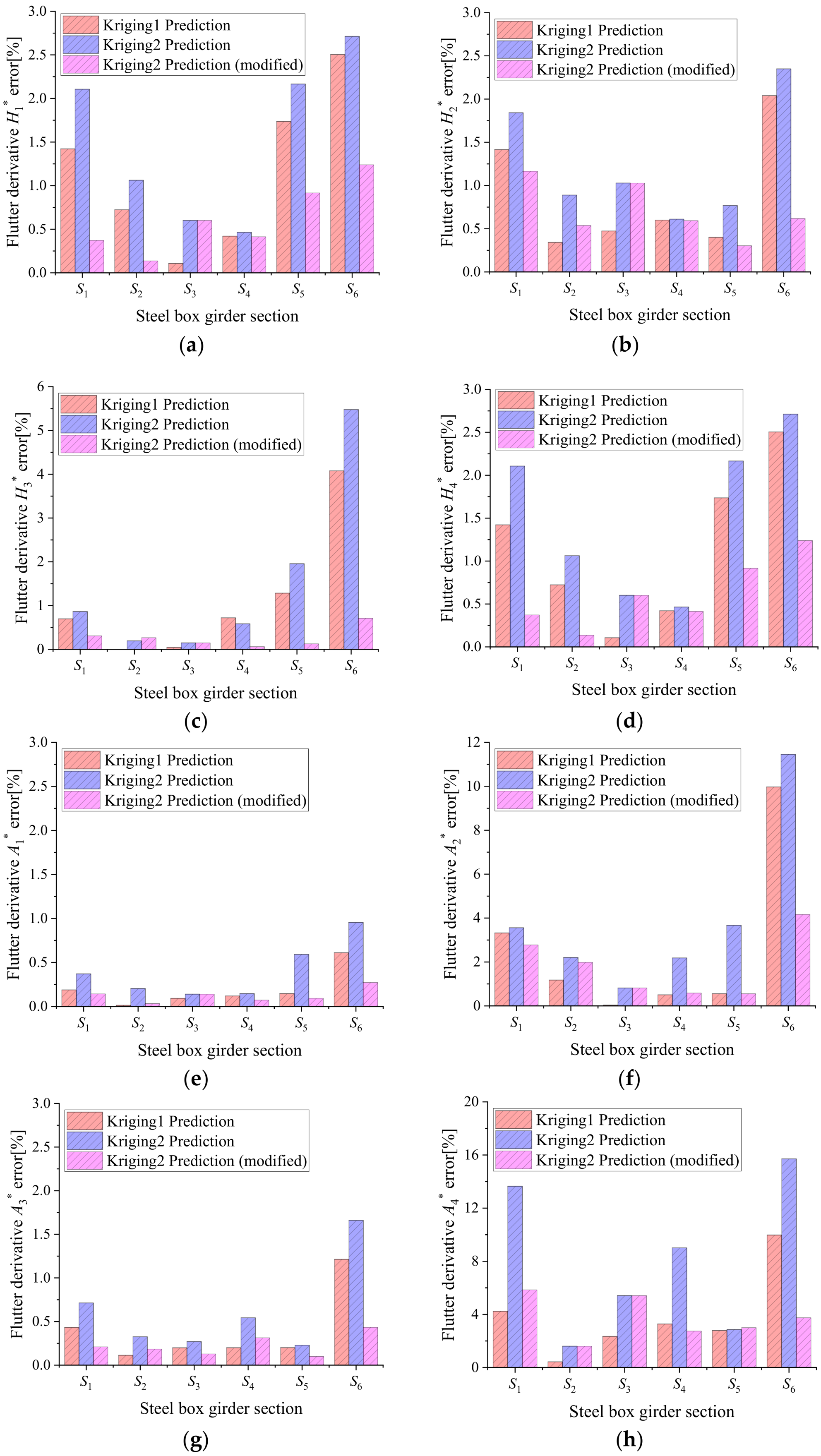

Figure 18. Prediction errors of flutter derivatives of steel box girders: (**a**) $H_1{}^*$; (**b**) H_2^*; (**c**) H_3^*; (**d**) H_4^* ; (**e**) A_1^*; (**f**) A_2^*; (**g**) A_3^*; (**h**) A_4^*.

5. Conclusions

It is known that the flutter characteristics of flat steel box girders are affected by the girder's cross-section shape. In order to find the most reasonable girder cross-section shape, wind tunnel tests are needed for various girder cross-sections. The workload is enormous, and the cost is huge. With the development of CFD numerical simulation technology, numerical wind tunnel based on CFD simulation has been applied and accepted in wind engineering. However, the consuming time in CFD modeling and calculation of all investigated girder cross-sections is vast.

In this paper, the kriging method is used to predict the flutter derivatives of flat steel box girders, which reduces a lot of repetitive modeling and calculation work and achieves good results. The predicted flutter derivatives are close to those obtained by CFD numerical simulations. Therefore, it is feasible to use the Kriging model to predict the flutter derivative of steel box girders. On this basis, it is concluded that the girder sections for training the Kriging model should be distributed uniformly in the section design domain. The prediction error of the Kriging model increases with the decrease of training samples. However, the improved Kriging model training method can effectively improve the prediction accuracy under a few training samples.

In the application of practical engineering, the process of predicting flutter derivatives can be divided into two stages. In the first stage, it is necessary to perform the verification both spatial and temporal for the CFD meshes and adjust the CFD model parameters according to the wind tunnel test results to realize the effectiveness of CFD numerical simulation. In the second stage, the Kriging predictions on flutter derivatives of flat steel box girders are performed based on the aerodynamic derivatives of a small number of cross-sections calculated by CFD numerical simulations. The main content of this paper is for the second stage to propose a data-driven prediction method based on the Kriging model to predict flutter derivatives of the bridge deck section, while the verification involved in the first stage was not considered due to the lack of wind tunnel test data in this paper. However, it needs to perform the verification in practical application, which will be analyzed in the following research.

Author Contributions: Conceptualization, J.L. and C.L.; methodology, Z.Q.; software, Y.Z. and Z.Q.; validation, J.L., Z.Q. and L.C.; formal analysis, Y.Z. and Z.Q.; investigation, Z.Q. and L.C.; resources, J.L.; data curation, Y.Z.; writing—original draft preparation, Y.Z.; writing—review and editing, J.L., Z.Q. and C.L.; visualization, L.C.; supervision, C.L.; project administration, J.L.; funding acquisition, J.L. All authors have read and agreed to the published version of the manuscript.

Funding: This research was funded by the National Natural Science Foundation of China, grant number 11962006.

Institutional Review Board Statement: Not applicable.

Informed Consent Statement: Not applicable.

Data Availability Statement: Not applicable.

Conflicts of Interest: The authors declare no conflict of interest.

References

1. Larsen, A.; Wall, A. Shaping of bridge box girders to avoid vortex shedding response. *J. Wind Eng. Ind. Aerodyn.* **2012**, *104–106*, 159–165. [CrossRef]
2. Wang, H.; Tao, T.; Zhou, R.; Hua, X.; Kareem, A. Parameter sensitivity study on flutter stability of a long-span triple-tower suspension bridge. *J. Wind Eng. Ind. Aerodyn.* **2014**, *128*, 12–21. [CrossRef]
3. Zhao, G.; Li, Y.; Bai, H. Wind tunnel test and the analysis of buffeting performance of free-standing tower of cable-stayed bridge under yaw wind. *Adv. Mater. Res.* **2012**, *532–533*, 215–219. [CrossRef]
4. Larsen, A.; Larsose, G.L. Dynamic wind effects on suspension and cable-stayed bridges. *J. Sound Vib.* **2015**, *334*, 2–28. [CrossRef]
5. Larose, G.L.; Davenport, A.G.; King, J.P.C. Wind effects on long span bridges: Consistency of wind tunnel results. *J. Wind Eng. Ind. Aerodyn.* **1992**, *42*, 1191–1202. [CrossRef]

6. Diana, G.; Resta, F.; Zasso, A.; Belloli, M.; Rocchi, D. Forced motion and free motion aeroelastic tests on a new concept dynamometric section model of the Messina suspension bridge. *J. Wind Eng. Ind. Aerodyn.* **2004**, *92*, 441–462. [CrossRef]
7. Li, K.; Li, S.; Ge, Y.; Yan, B. Wind effects on long span bridges: An investigation into the bimodal flutter details based on flutter derivatives' contribution along the bridge deck's surface. *J. Wind Eng. Ind. Aerodyn.* **2019**, *192*, 1–16. [CrossRef]
8. Sarwar, M.W.; Ishihara, T.; Shimada, K.; Yamasaki, Y.; Ikeda, T. Prediction of aerodynamic characteristics of a box girder bridge section using the LES turbulence model. *J. Wind Eng. Ind. Aerodyn.* **2008**, *96*, 1895–1911. [CrossRef]
9. Mannini, C.; Šoda, A.; Voß, R.; Schewe, G. Unsteady RANS simulations of flow around a bridge section. *J. Wind Eng. Ind. Aerodyn.* **2010**, *98*, 742–753. [CrossRef]
10. Šarkić, A.; Fisch, R.; Höffer, R.; Bletzinger, K.U. Bridge flutter derivatives based on computed, validated pressure fields. *J. Wind Eng. Ind. Aerodyn.* **2012**, *104–106*, 141–151. [CrossRef]
11. Ge, Y.; Xiang, H. Computational models and methods for aerodynamic flutter of long-span bridges. *J. Wind Eng. Ind. Aerodyn.* **2008**, *96*, 1912–1924. [CrossRef]
12. Nagao, F.; Utsunomiya, H.; Oryu, T.; Manabe, S. Aerodynamic efficiency of triangular fairing on box girder bridge. *J. Wind Eng. Ind. Aerodyn.* **1993**, *49*, 565–574. [CrossRef]
13. Montoya, M.C.; Nieto, F.; Hernandez, S.; Kusano, I.; Alvarez, A.J.; Jurado, J.A. CFD-based aeroelastic characterization of streamlined bridge deck cross-sections subject to shape modifications using surrogate models. *J. Wind Eng. Ind. Aerodyn.* **2018**, *177*, 405–428. [CrossRef]
14. Farsani, H.Y.; Valentine, D.T.; Arena, A.; Lacarbonara, W.; Marzocca, P. Indicial functions in the aeroelasticity of bridge decks. *J. Fluid Struct.* **2014**, *48*, 203–215. [CrossRef]
15. Arena, A.; Lacarbonara, W.; Valentine, D.T.; Marzocca, P. Aeroelastic behavior of long-span suspension bridges under arbitrary wind profiles. *J. Fluid Struct.* **2014**, *50*, 105–119. [CrossRef]
16. Yang, Y.; Lu, H.; Tan, X.; Chai, H.K.; Wang, R.; Zhang, Y. Fundamental mode shape estimation and element stiffness evaluation of girder bridges by using passing tractor-trailers. *Mech. Syst. Signal Process.* **2022**, *169*, 108746. [CrossRef]
17. Yang, Y.; Zhang, Y.; Tan, X. Review on Vibration-Based Structural Health Monitoring Techniques and Technical Codes. *Symmetry* **2021**, *13*, 1998. [CrossRef]
18. Yang, Y.; Ling, Y.; Tan, X.; Wang, S.; Wang, R. Damage identification of frame structure based on approximate Metropolis–Hastings algorithm and probability density evolution method. *Int. J. Struct. Stab. Dyn.* **2022**, *22*, 2240014. [CrossRef]
19. Scanlan, R.H.; Tomko, J.J. Airfoil and bridge deck flutter derivatives. *J. Eng. Mech. ASCE* **1971**, *97*, 1717–1737. [CrossRef]
20. Lacarbonara, W.; Arena, A. Flutter of an arch bridge via a fully nonlinear continuum formulation. *J. Aerospace Eng.* **2011**, *24*, 112–123. [CrossRef]
21. Arena, A.; Lacarbonara, W. Nonlinear parametric modeling of suspension bridges under aeroelastic forces: Torsional divergence and flutter. *Nonlinear Dyn.* **2012**, *70*, 2487–2510. [CrossRef]
22. Sarkar, P.P.; Jones, N.P.; Scanlan, R.H. Identification of aeroelastic parameters of flexible bridges. *J. Eng. Mech.* **1994**, *120*, 1718–1742. [CrossRef]
23. Cui, Y.; Chen, G. Simulations for identification of flutter derivatives of bridge section using the coupled-forced-vibration method. *J. Vib. Eng.* **2007**, *20*, 35–39.
24. Chen, C.H.; Wu, J.C.; Chen, J.H. Prediction of flutter derivatives by artificial neural networks. *J. Wind Eng. Ind. Aerodyn.* **2008**, *96*, 1925–1937. [CrossRef]
25. Elshaer, A.; Bitsuamlak, G.; El Damatty, A. Enhancing wind performance of tall buildings using corner aerodynamic optimization. *Eng. Struct.* **2017**, *136*, 133–148. [CrossRef]
26. Gao, Y.; Turng, L.S.; Wang, X. Adaptive geometry and process optimization for injection molding using the kriging surrogate model trained by numerical simulation. *Adv. Polym. Technol.* **2008**, *27*, 1–16. [CrossRef]
27. Durmaz, M.; Karslioglu, M.O.; Nohutcu, M. Regional VTEC modeling with multivariate adaptive regression splines. *Adv. Space Res.* **2010**, *46*, 180–189. [CrossRef]
28. Liu, H.; Antar, Y.M.M.; Wu, Z. A model of an artificial neural network for frequency dependence of radar cross section. *Microw. Opt. Technol. Lett.* **1999**, *20*, 315–318. [CrossRef]
29. Bernardini, E.; Spence, S.M.J.; Wei, D.; Kareem, A. Aerodynamic shape optimization of civil structures: A CFD-enabled Kriging-based approach. *J. Wind Eng. Ind. Aerodyn.* **2015**, *144*, 154–164. [CrossRef]
30. Forrester, A.I.J.; Sóbester, A.; Keane, A.J. *Engineering Design via Surrogate Modelling. A Practical Guide*; John Wiley and Sons Ltd.: Hoboken, NJ, USA, 2008.
31. Jones, D.R. A taxonomy of global optimization methods based on response surfaces. *J. Glob. Optim.* **2001**, *21*, 345–383. [CrossRef]